JOURNAL OF PROPULSION AND POWER
Vol. 10, No. 4, July–Aug. 1994

Assumed Joint Probability Density Function Approach for Supersonic Turbulent Combustion

R. A. Baurle,* G. A. Alexopoulos,* and H. A. Hassan†
North Carolina State University, Raleigh, North Carolina 27695

In a recent experiment, Cheng et al. used uv spontaneous vibrational Raman scattering and laser-induced predissociative fluorescence techniques for simultaneous measurements of temperature and concentrations of O_2, H_2, H_2O, OH, and N_2 (and the rms of their fluctuations) in supersonic turbulent reacting shear layers. Because present computational techniques are not suited for the prediction of all of the above measurements, a new approach has been developed and is being used to predict all relevant flow properties and the rms of their fluctuations (where appropriate). The approach explores the use of a multivariate Beta PDF for concentrations. In particular, a version developed by Girimaji to model scalar mixing in turbulent flows is employed. Predictions using this model were, in general, satisfactory in regions preceding ignition, but not in regions downstream of ignition. Part of the discrepancy is a result of our current inability to relate Favre and time averages.

Nomenclature

C_Q = turbulent model constant for Q
D = molecular diffusion coefficient
D_t = turbulent diffusion coefficient
k = turbulent kinetic energy
l = width of the mixing layer
ns = number of chemical species
$P_1(T)$ = probability density function for temperature
$P_2(Y_k)$ = probability density function for mass fractions
Q = species variance sum
S = sum of the square of mean mass fraction
T = temperature
u_j = velocity components
x_j = spatial coordinates
Y_k = species mass fractions
β_k = multivariate Beta PDF parameters
Γ = gamma function
δ = Dirac delta function
ρ = density
τ = turbulent time scale
$\dot{\omega}_k$ = species production rates

Subscripts
i, j = spatial coordinates
k, m = species number
t = turbulent quantity

Superscripts
$\bar{}$ = time-averaged quantity
$'$ = fluctuating component
$\tilde{}$ = Favre-averaged quantity
$''$ = Favre fluctuating component

Presented as Paper 92-3844 at the AIAA/SAE/ASME/ASEE 28th Joint Propulsion Conference and Exhibit, Nashville, TN, July 6–8, 1992; received Oct. 13, 1992; revision received Nov. 16, 1993; accepted for publication Nov. 23, 1993.

*Research Assistant, Department of Mechanical and Aerospace Engineering, Box 7910.
†Professor, Department of Mechanical and Aerospace Engineering, Box 7910.

Introduction

THE successful design of scramjet engines requires the understanding of turbulent mixing and its effect on combustion at supersonic speeds. The major handicap for developing codes that are capable of predicting flowfields in such engines is a lack of availability of accurate measurements in flow conditions representative of scramjet flows. Using the flow in a supersonic reacting shear layer, Cheng et al.[1] presented detailed and simultaneous measurements of temperature and concentrations of O_2, H_2, H_2O, OH, and N_2 along with the rms of their fluctuations. These quantities were measured using uv spontaneous vibrational Raman scattering and laser-induced predissociative fluorescence techniques with a spatial resolution of 0.4 mm. Measurements such as these provide the modeler with an opportunity to develop and test models that will eventually be used for the design of scramjet engines.

Ideally, one would like to use an approach based on the probability density function (PDF) developed by Pope.[2] Un-

Table 1 Chemistry model

Reaction	A	b	T_a
$H_2 + O_2 \rightarrow OH + OH$	0.170E + 14	0.00	24,157.0
$H + O_2 \rightarrow OH + O$	0.120E + 18	−0.91	8,310.5
$OH + H_2 \rightarrow H_2O + H$	0.220E + 14	0.00	2,591.8
$O + H_2 \rightarrow OH + H$	0.506E + 05	2.67	3,165.6
$OH + OH \rightarrow H_2O + O$	0.630E + 13	0.00	548.6
$H + OH + M \rightarrow H_2O + M$	0.221E + 23	−2.00	0.0
$H + H + M \rightarrow H_2 + M$	0.730E + 18	−1.00	0.0

Units of A are a multiple of $cm^3 \cdot mole^{-1} \cdot s^{-1}$.

Table 2 Exit conditions

Exit conditions	Hydrogen jet	Outer jet	Ambient air
Mach number	1	2	0
Temperature, K	545	1250	300
Velocity, m/s	1780	1417	0
Pressure, MPa	0.112	0.107	0.101
Mass fraction			
Y_{H_2}	1.0	0.0	0.0
Y_{O_2}	0.0	0.245	0.233
Y_{N_2}	0.0	0.58	0.757
Y_{H_2O}	0.0	0.175	0.01

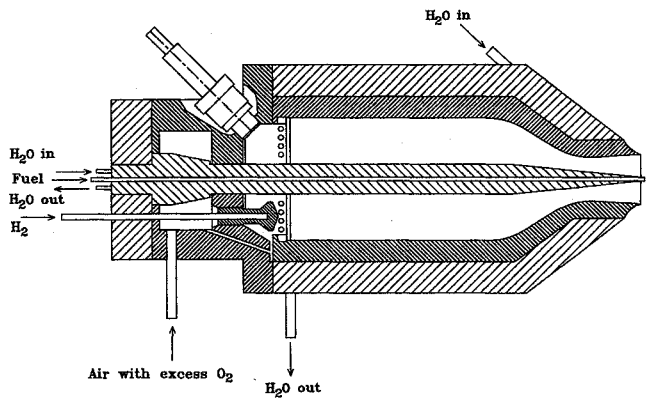

Fig. 1 Schematic of test apparatus.

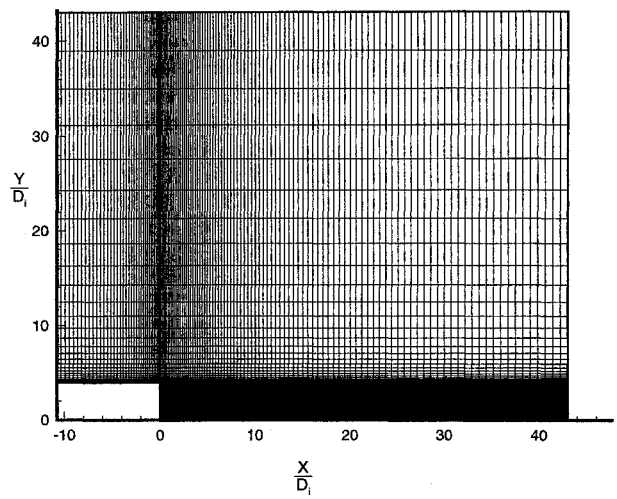

Fig. 2 Computational grid.

fortunately, the equations developed by Pope are not suited for describing supersonic combustion. Moreover, the computational effort associated with such an implementation is so great that, at present, the approach is not a viable engineering tool. Because of this, an assumed PDF approach will be employed. Obviously, such an approach is not as elegant as that of Ref. 2. However, it does have the potential of being developed into a viable engineering tool.

The objective of this investigation is to develop such an approach. It is obvious that approaches developed for low-speed flows[3] cannot be used for supersonic flows. Thus, a full kinetic model is required. Here, we are using an abridged version of the Jachimowski model[4] which consists of seven reactions (Table 1) and allows for the presence of O_2, H_2, H_2O, OH, O, H, and an inert species N_2. In order to allow for the effects of fluctuations of concentrations on reactions, it is necessary to develop a class of joint PDFs that are capable of describing such fluctuations. A first step in this direction was proposed by Girimaji[5] who developed a multivariate Beta PDF to study multiple scalar mixing in turbulent flows. In this model, all species variances and covariances can be determined once the mean quantities and one scalar quantity (the sum of the species variances) are known. Such a joint PDF has both positive and negative aspects. On the plus side, only one additional field equation for the sum of the species variances needs to be modeled and integrated in conjunction with the other equations. This makes it possible to incorporate the effects of concentration fluctuations on the turbulent flowfield with a minimum of computational effort. On the negative side, one would expect the variances and covariances to be somewhat independent which would require more than one field equation to describe them. Thus, one is led to believe that this joint PDF has a limited range of applicability. Therefore, determination of the limitations of this PDF is one of the major goals of this work. Another potential problem can be traced to compressibility effects. In compressible flow computations, Favre averaging is commonly used. Use of the joint PDF of Ref. 5 introduces time averages. The relationship between the two types of averaging on a quantity ϕ is given by

$$\tilde{\phi} = \bar{\phi} + (\overline{\rho'\phi'}/\bar{\rho}) \tag{1}$$

When ϕ is a vector, a gradient diffusion approximation can be used to model $\overline{\rho'\phi'}$. It is not clear how to model this term when ϕ is a scalar. However, if $\rho = \rho(T, Y_k)$ is known a priori, then the expression

$$\overline{\rho Y_k} = \int \rho Y_k P(T, Y_k, \quad x_j)\, dY_k\, dT = \bar{\rho}\tilde{Y}_k \tag{2}$$

can be used to obtain a Favre average. Unfortunately, this would require the assumption of a constant pressure; an assumption that is not invoked here. As a result, we are forced in the following development to ignore the differences between Favre and time averages when ϕ is a scalar.

Joint PDF

The species production rates are functions of temperature and composition. Thus, in order to evaluate their averages, a joint PDF involving both temperature and composition is needed. In this work, the joint PDF was chosen as

$$P(T, Y_k) = P_1(T)P_2(Y_k) \tag{3}$$

Here, $P_1(T)$ was chosen as a Gaussian distribution

$$P_1(T) = (1/\sqrt{2\pi\overline{T''^2}})\exp\{-[(T - \tilde{T})^2/2\overline{T''^2}]\} \tag{4}$$

and $P_2(Y_k)$ was chosen as the multivariate Beta distribution function developed by Girimaji[5]

$$P_2(Y_k) = \left[\Gamma\left(\sum_{k=1}^{ns}\beta_k\right)\Big/\prod_{k=1}^{ns}\Gamma(\beta_k)\right] \times \left[\delta\left(1 - \sum_{k=1}^{ns} Y_k\right)\prod_{k=1}^{ns} Y_k^{\beta_k - 1}\right] \tag{5}$$

where Y_k is the mass fraction of species k which obeys the relation

$$\sum_{k=1}^{ns} Y_k = 1 \tag{6}$$

It can be shown that[5]

$$\beta_k = \tilde{Y}_k\{[(1 - S)/Q] - 1\} \equiv \tilde{Y}_k(\sigma - 1) \tag{7}$$

where

$$S = \sum_{k=1}^{ns} (\tilde{Y}_k)^2$$
$$Q = \sum_{k=1}^{ns} \overline{Y_k''^2} \tag{8}$$

Moreover

$$\overline{Y_k'' Y_m''} = [(\tilde{Y}_m \delta_{km} - \tilde{Y}_k \tilde{Y}_m)/\sigma] \tag{9}$$

In the above expression, $\delta_{km} = 1$ if $k = m$ and is zero otherwise.

The special nature of the above model can be seen from Eq. (9) which shows that all variances and covariances are determined once the means and the sum of all variances are known. Moreover, all covariances are negative. Because the mean quantities are determined from governing equations, only an additional field equation for Q is needed to determine all parameters that appear in the assumed multivariate Beta PDF. The Favre-averaged Navier-Stokes equations together with the species conservation equations, transport properties, and chemistry model are described in Ref. 6. The equation governing the enthalpy variance is described in Refs. 7 and 8. The equation governing Q has a form similar to that of the enthalpy variance, and is given by[9]

$$\frac{\partial(\bar{\rho}\tilde{Q})}{\partial t} + \frac{\partial(\bar{\rho}\tilde{u}_j\tilde{Q})}{\partial x_j} = \frac{\partial}{\partial x_j}\left(\bar{\rho}D\frac{\partial \tilde{Q}}{\partial x_j} - \sum_{k=1}^{ns}\overline{\rho u_j'' Y_k''^2}\right) + 2\sum_{k=1}^{ns}\left(-\overline{\rho u_j'' Y_k''}\frac{\partial \tilde{Y}_k}{\partial x_j} - \bar{\rho}D\frac{\overline{\partial Y_k''}\,\overline{\partial Y_k''}}{\partial x_j \partial x_j} + \overline{\dot{\omega}_k Y_k''}\right) \tag{10}$$

where the turbulent terms are modeled as

$$-\sum_{k=1}^{ns}\overline{\rho u_j'' Y_k''^2} = \bar{\rho}D_t\frac{\partial \tilde{Q}}{\partial x_j}$$

$$-\overline{\rho u_j'' Y_k''} = \bar{\rho}D_t\frac{\partial \tilde{Y}_k}{\partial x_j} \tag{11}$$

$$\sum_{k=1}^{ns}\bar{\rho}D\frac{\overline{\partial Y_k''}\,\overline{\partial Y_k''}}{\partial x_j \partial x_j} = \bar{\rho}\frac{C_Q\tilde{Q}}{2\tau}$$

It is to be noted that the chemical source term $\overline{\dot{\omega}_k Y_k''}$ does not require modeling. It is directly calculated from the assumed PDF.

Results and Discussion

The turbulence model employed is the one-equation model developed in Ref. 8. For this case, the τ used in Eq. (10) is given by

$$\tau = (l/\sqrt{\tilde{k}}) \tag{12}$$

In addition, the constant C_Q employed in Eq. (11) was chosen as $\frac{1}{4}$, and the turbulent Lewis number was chosen as 1.

The chemistry model employed is shown in Table 1. A schematic diagram of the supersonic burner is given in Fig. 1, and the burner exit conditions are summarized in Table 2. All calculations (unless otherwise specified) were carried out using a 93 × 93 grid on a domain of 4 × 4 in. (≈43 i.d.) with a 37 × 29 block grid added to the ambient inflow boundary as shown in Fig. 2.

The present calculations assume that time-averaged scalars are essentially equal to the Favre-averaged scalars. Because of this, it is necessary to have an independent means of testing the model without introducing the above uncertainty. This can be accomplished by comparing Eq. (9) with the measurements of Ref. 1, which used time averaging. The means and the sum of the variances were calculated from experiment, and Eq. (9) was then used to calculate the species variances. The resulting values are compared with the experimental values in Figs. 3–7, at the 1- and 4-in. axial stations. In the experiment, ignition takes place just downstream of the 1-in.

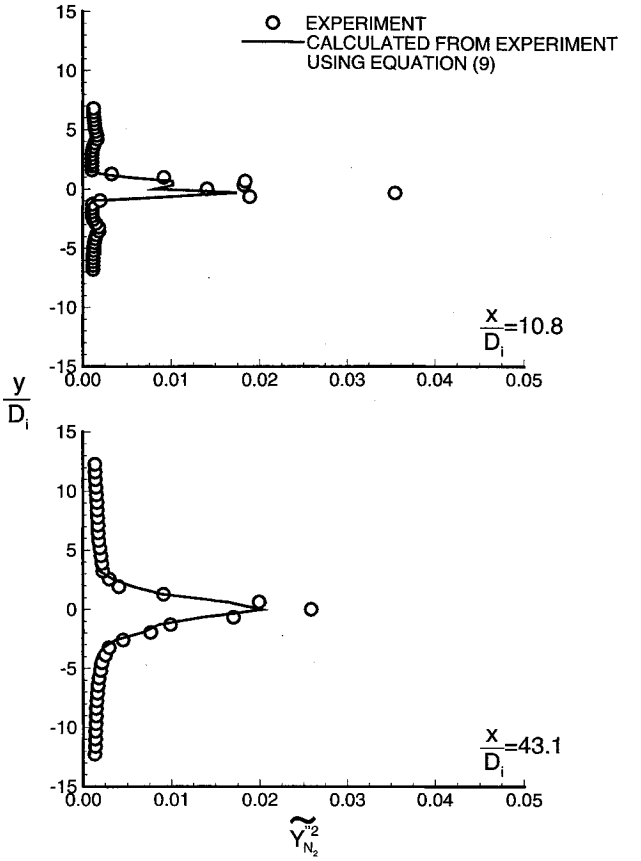

Fig. 3 N_2 mass fraction variance comparisons between model and experiment.

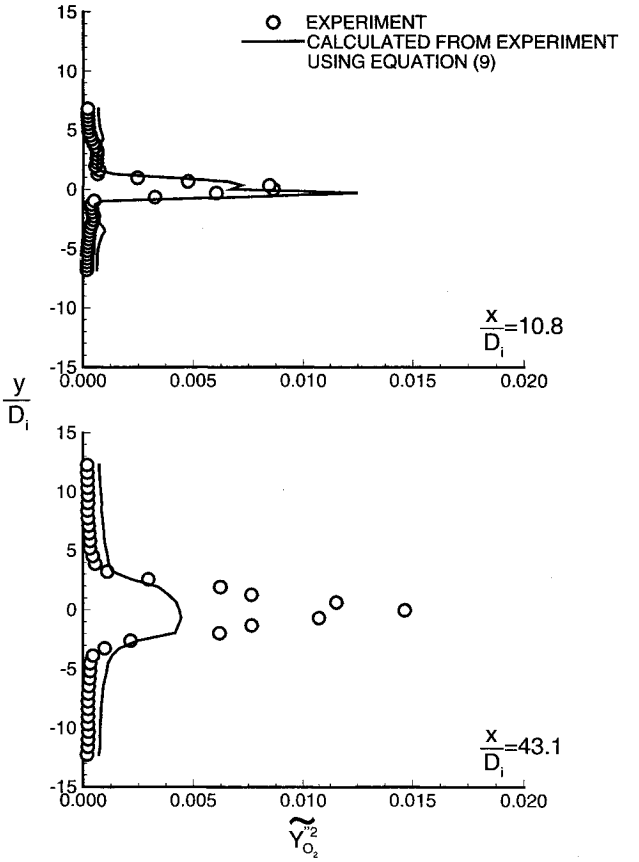

Fig. 4 O_2 mass fraction variance comparisons between model and experiment.

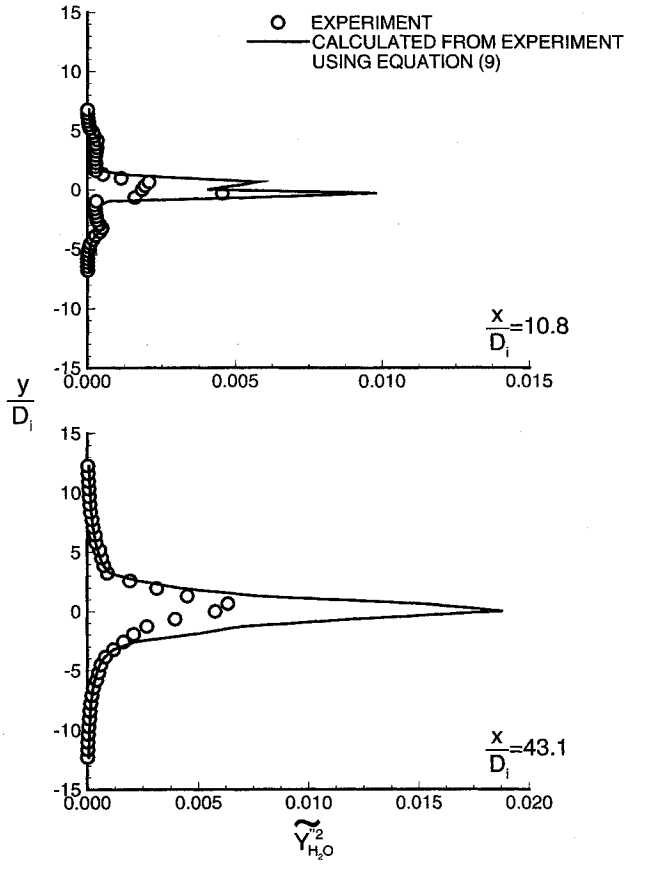

Fig. 5 H_2O mass fraction variance comparisons between model and experiment.

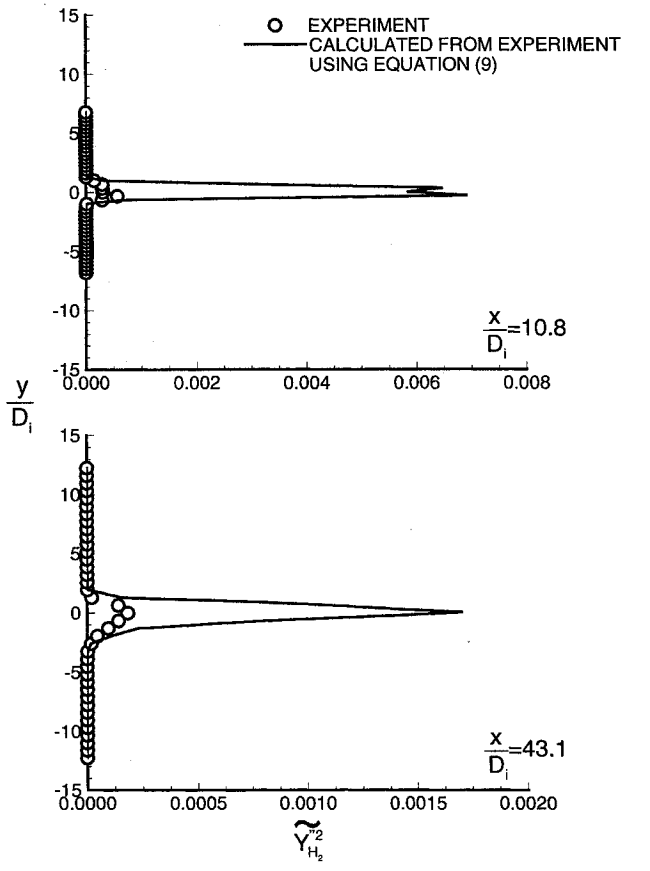

Fig. 6 H_2 mass fraction variance comparisons between model and experiment.

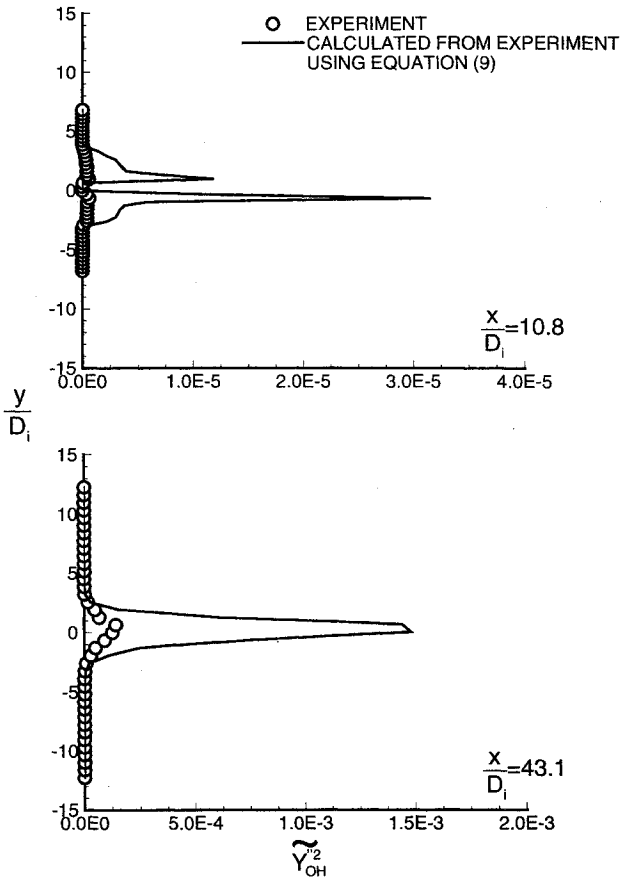

Fig. 7 OH mass fraction variance comparisons between model and experiment.

station. As seen from the figures, qualitative agreement is indicated at the 1-in. station (before ignition) for the major species and for N_2 at the 4-in. station. This shows that the assumed PDF gives adequate agreement in regions where combustion has not taken place and for the inert species. In all other situations, the agreement is somewhat inadequate. It should be noted that because of a slight device misalignment,[1] the experimental data is not completely symmetric.

The next set of figures (Figs. 8 and 9) compare results of calculation, with and without the use of the PDF, to experiment. For most of the mean flow variables the differences were negligible, so only comparisons of mean temperature and OH mole fraction are shown here. It is noted that the results with the PDF did show some improvements when compared to experiment. These figures also show that ignition is predicted to start closer to the exit of the burner when the PDF is employed.

One of the advantages of using a PDF formulation is that all averages involving the chemical source terms can be calculated directly. However, the source term $\overline{\dot{\omega}_k Y_k''}$ appearing in Eq. (10) contains third- and fourth-order correlations. Since second-order correlations were not predicted well in regions of combustion (from Figs. 3–7), it was felt that the resulting expression may not be very accurate. Thus, another set of calculations were carried out with the chemical source term set to zero.

Figures 10–13 compare the calculated and measured variances. As seen from the figures, both sets of calculations yield similar results at the 1-in. station (because the chemical source term is negligible here), and departures are seen at the downstream stations. Better agreement with experiment is indicated when the chemical source term is set equal to zero in Eq. (10). In an effort to explain this behavior, attention

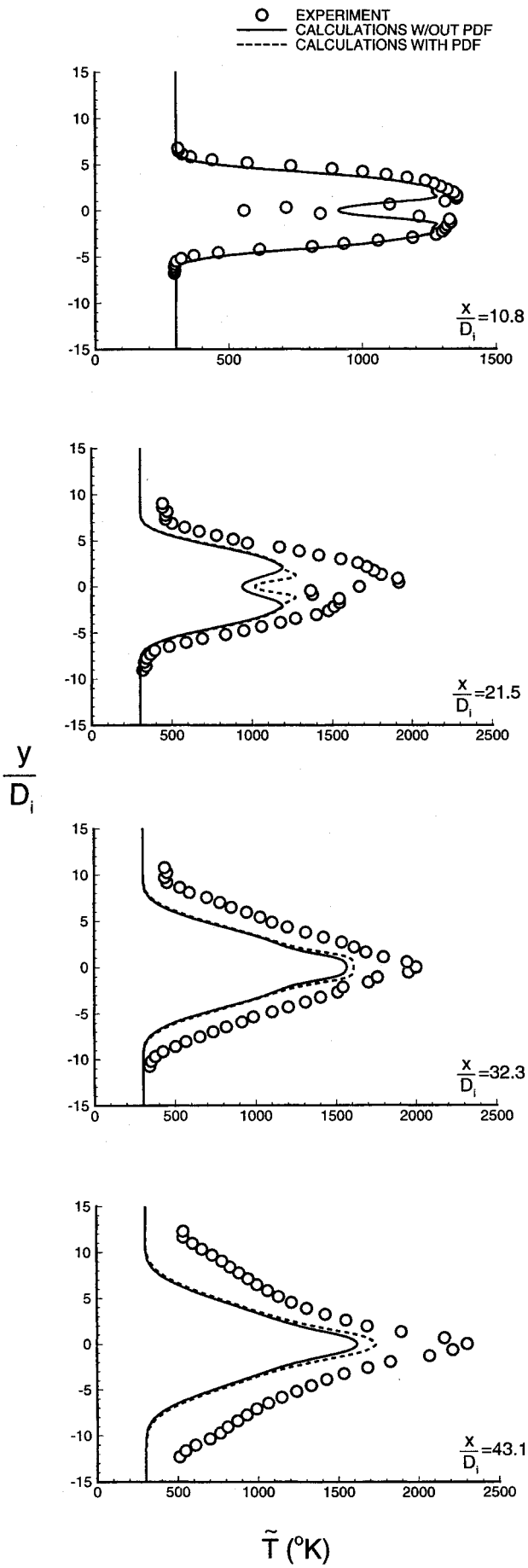

Fig. 8 Computed mean temperature profiles with and without the PDF compared with experiment.

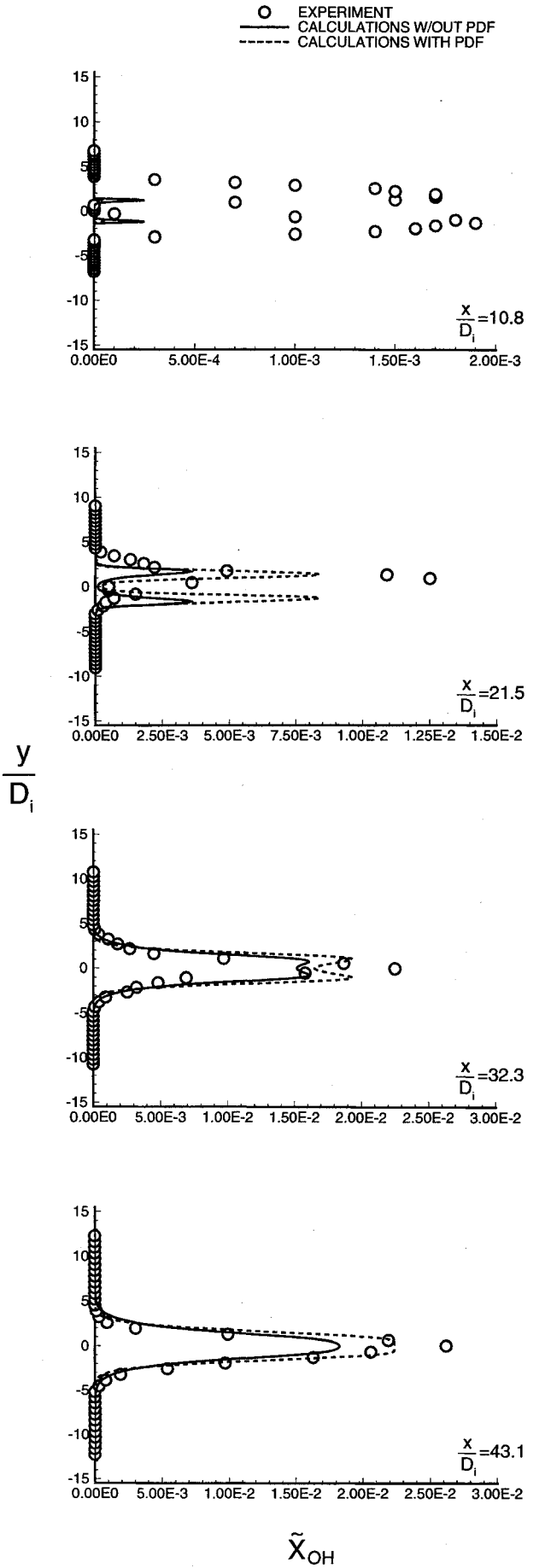

Fig. 9 Computed mean OH mole fraction profiles with and without the PDF compared with experiment.

is focused on Fig. 14, which plots the dominant source terms on the right side of Eq. (10). As seen from this figure, the chemical source term consistently acts as a dissipation term, which is small in the early stages of combustion, but becomes the dominant dissipation term in the latter stages. Thus, the effect of this term is to reduce the variance ($\tilde{Q}$) which effectively eliminates the fluctuations of the species mass fractions. This same conclusion was drawn by Narayan and Girimaji[10] using the same multivariate Beta PDF. This drastic reduction in the variances was not seen in the experimental data. This suggests that either Eq. (10) is missing additional terms or that the inaccuracies in the higher-order moments appearing in the chemical source term are such that the accuracy of the entire term is questionable. The missing terms in Eq. (10) may be a result of the assumption that Favre and time averages are set equal. Since

$$\tilde{Y}_k = \bar{Y}_k + (\overline{\rho' Y_k'}/\bar{\rho}) \tag{13}$$

the term $\overline{\rho' Y_k'}$, which is a scalar, is expected to increase with an increase in the turbulent Mach number. To the best of our knowledge, there is no accepted way of modeling this term. Therefore, it is difficult to assess the assumption regarding the averaging. Similarly, it is difficult to assess inaccuracies contributed by the higher-order correlations on the chemical source term. Based on the above considerations, it is not clear why removing the chemical source term in Eq. (10) gives better agreement with experiment. For the time being, such a result should be considered as a direct consequence of an

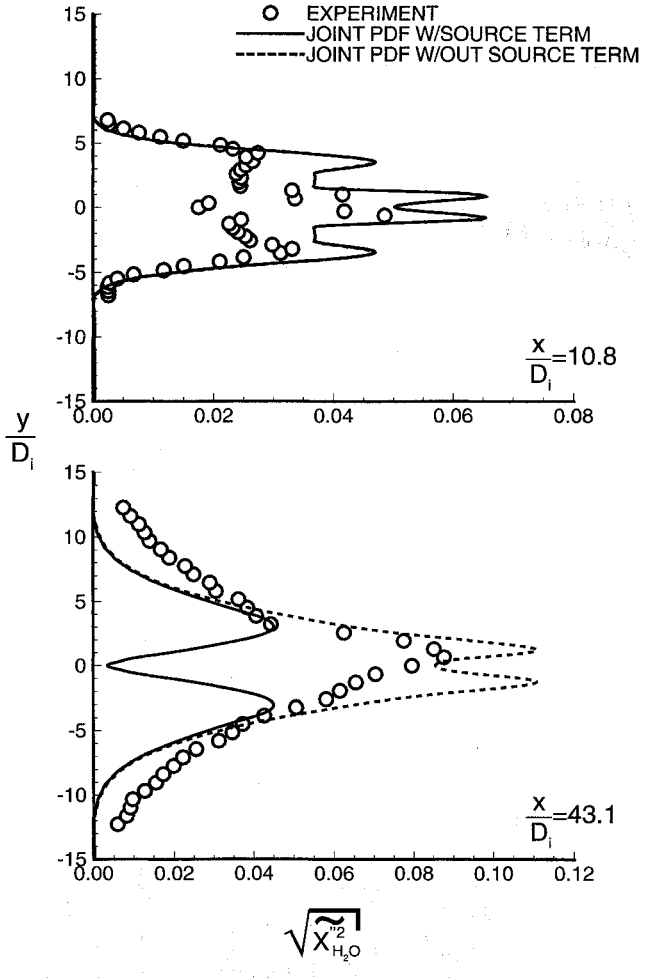

Fig. 10 Computed rms H_2O mole fraction profiles with and without the chemical source term compared with experiment.

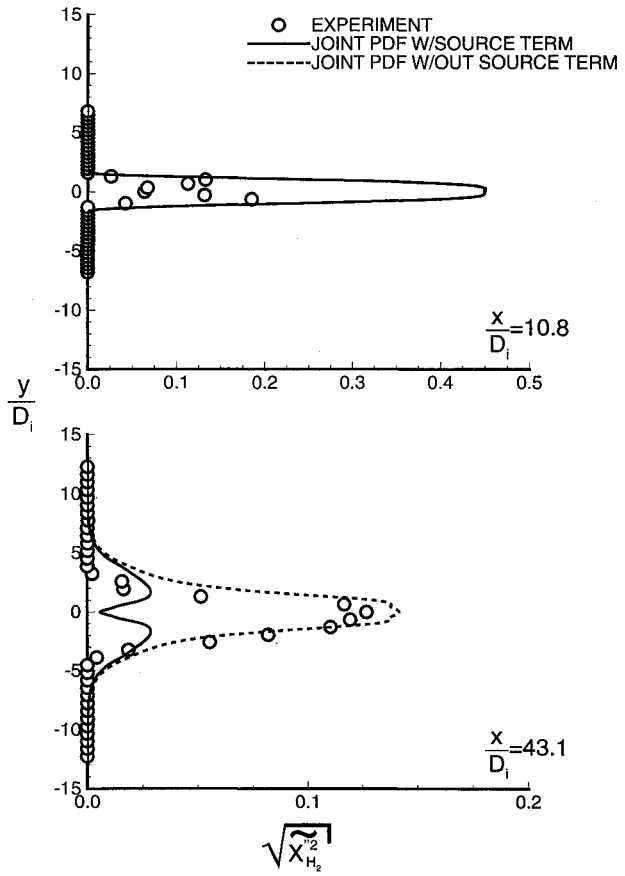

Fig. 11 Computed rms H_2 mole fraction profiles with and without the chemical source term compared with experiment.

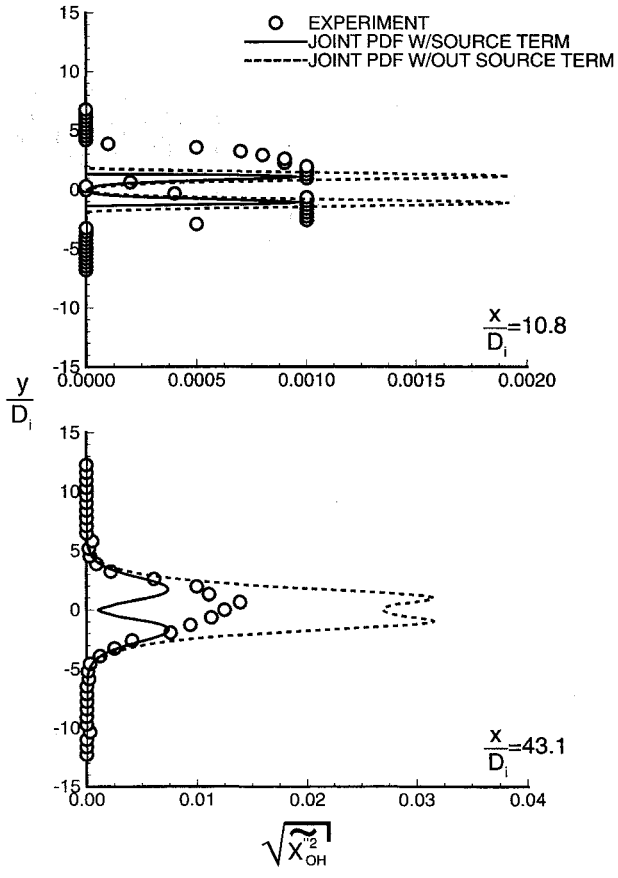

Fig. 12 Computed rms OH mole fraction profiles with and without the chemical source term compared with experiment.

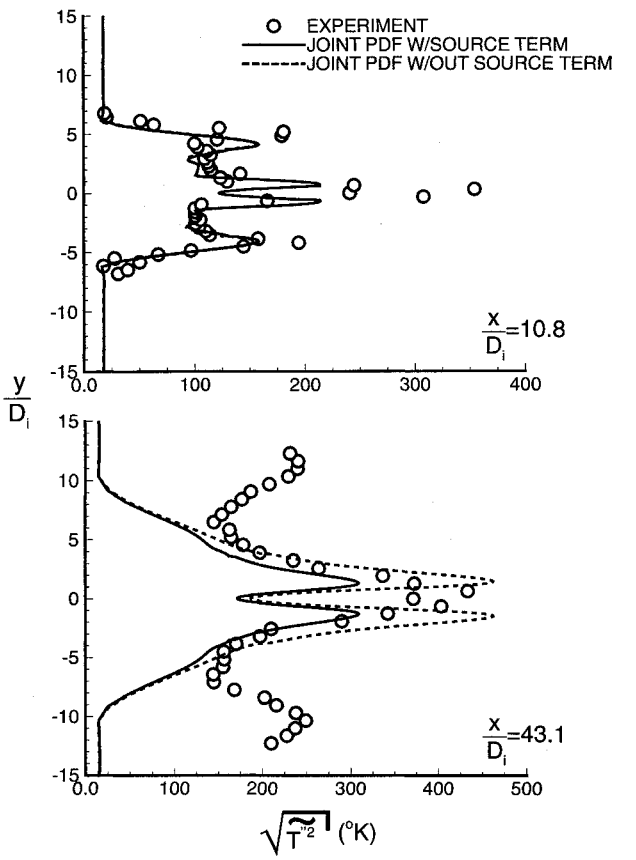

Fig. 13 Computed rms temperature profiles with and without the chemical source term compared with experiment.

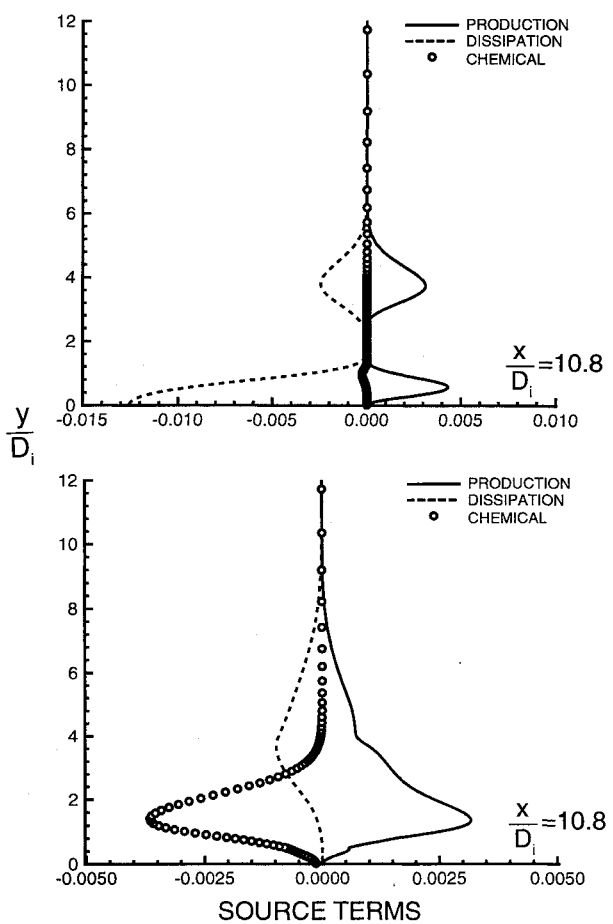

Fig. 14 Dominant source terms of the transport equation for $\tilde{Q}$.

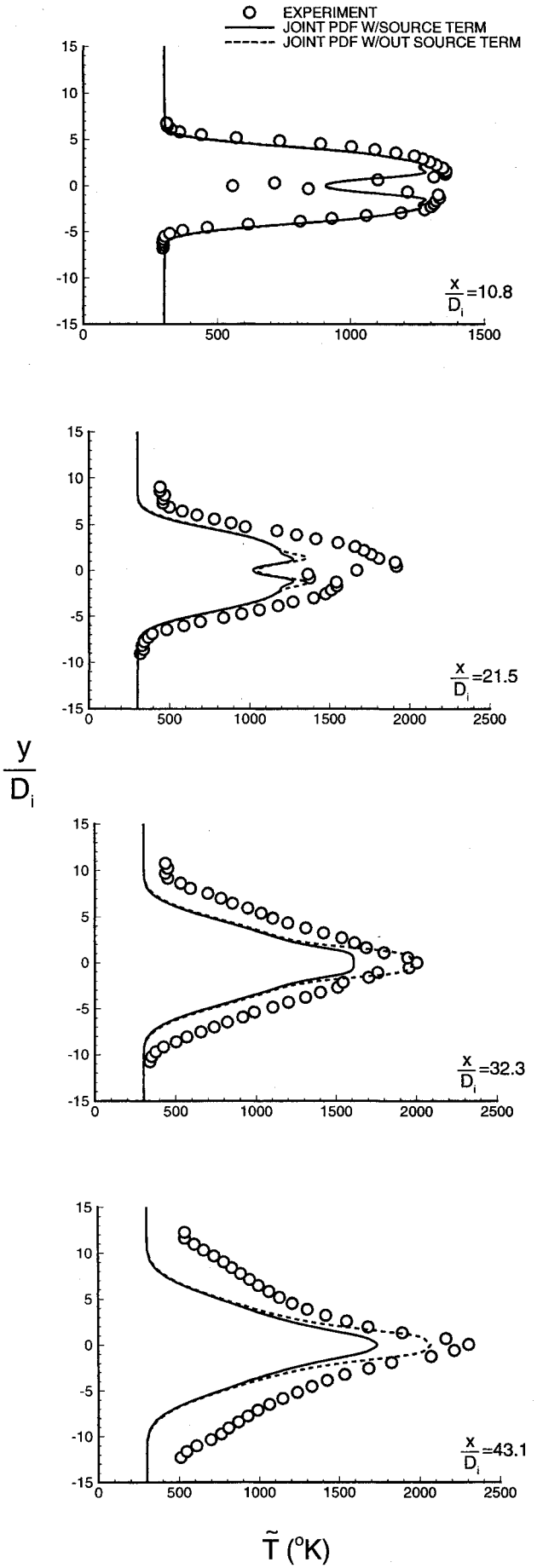

Fig. 15 Computed mean temperature profiles with and without the chemical source term compared with experiment.

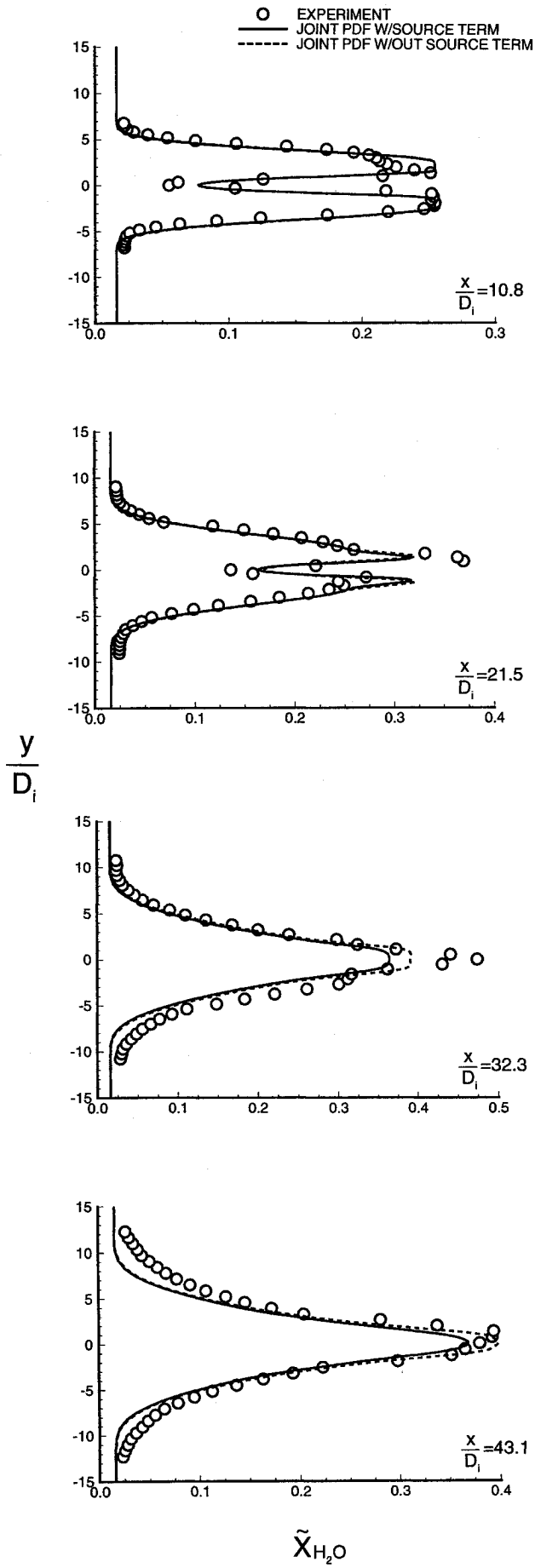

Fig. 16 Computed mean H_2O mole fraction profiles with and without the chemical source term compared with experiment.

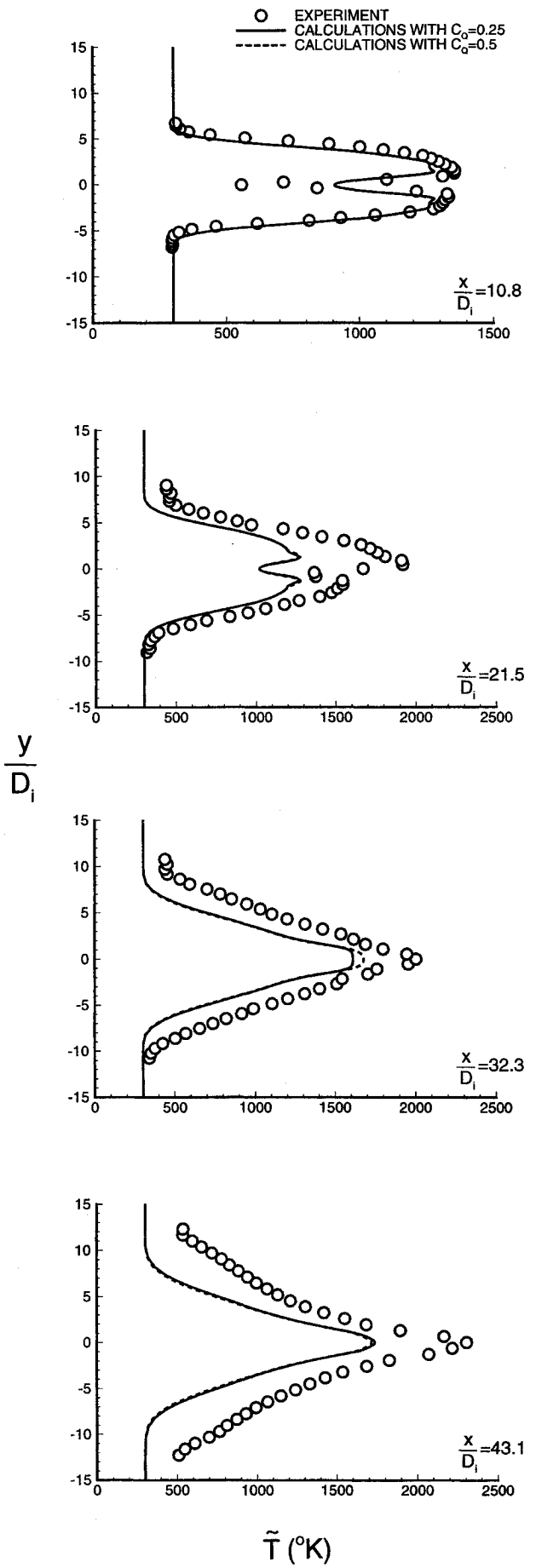

Fig. 17 Computed mean temperature profiles for various values of C_Q compared with experiment.

empirical assumption. Figures 15 and 16 compare calculated and measured mean temperature and H_2O mole fraction profiles. Again, better agreement is seen when the chemical source term is set equal to zero in Eq. (10). Similar results are indicated for the remaining species.

In an effort to determine if this effect can be explained, several other computations were performed to examine the sensitivity of the solution to the model constant C_Q, the turbulent Lewis number, initial turbulent intensity within the nozzle, and grid refinement. Figure 17 shows the model constant C_Q to have little effect on the mean temperature. As for the variances, Fig. 18 shows C_Q to have an influence preceding combustion; however, in regions of combustion its effect was minimal, which is consistent with the energy budget shown in Fig. 14.

Figures 19 and 20 show the effect of varying the turbulent Lewis number. As is seen from these figures, the turbulent Lewis number has little influence on the mean properties for values higher than 1, and a slightly larger effect for values less than 1. However, its effect on the variances is minimal when compared to the effects of the chemical source term $\overline{Y_k''\dot{\omega}_k}$.

The effect of the assumed initial turbulence intensity present in the nozzle is shown in Figs. 21 and 22. As seen from these figures, the solution is somewhat insensitive to the assumed turbulence intensity. Finally, Figs. 23 and 24 show comparisons with a more refined 121 × 121 grid on a domain of 4.5 × 3.5 in., showing the 93 × 93 grid to adequately resolve the flowfield.

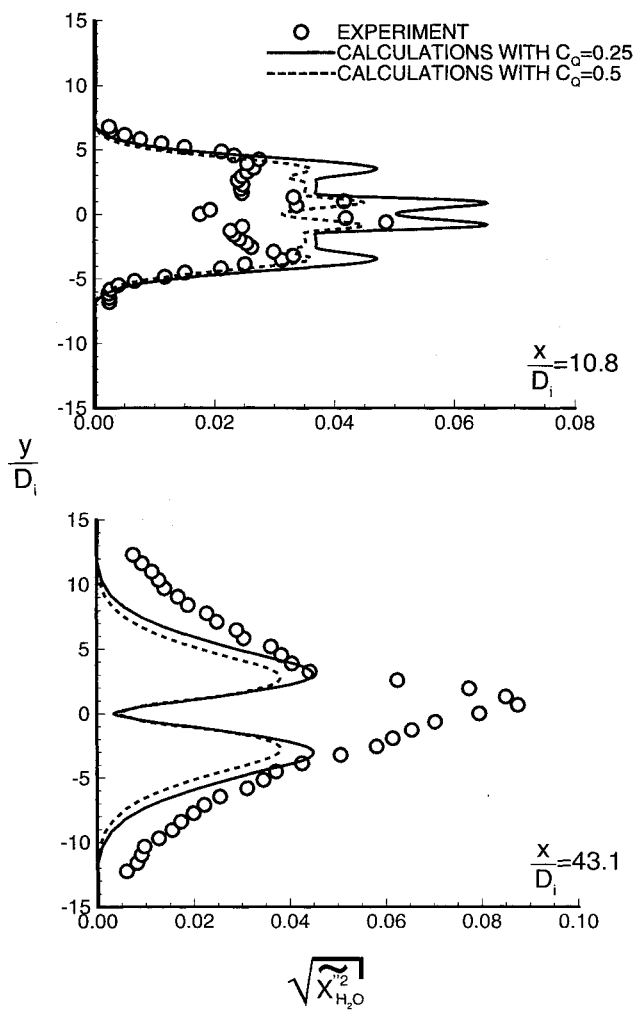

Fig. 18 Computed rms H_2O mole fraction profiles for various values of C_Q compared with experiment.

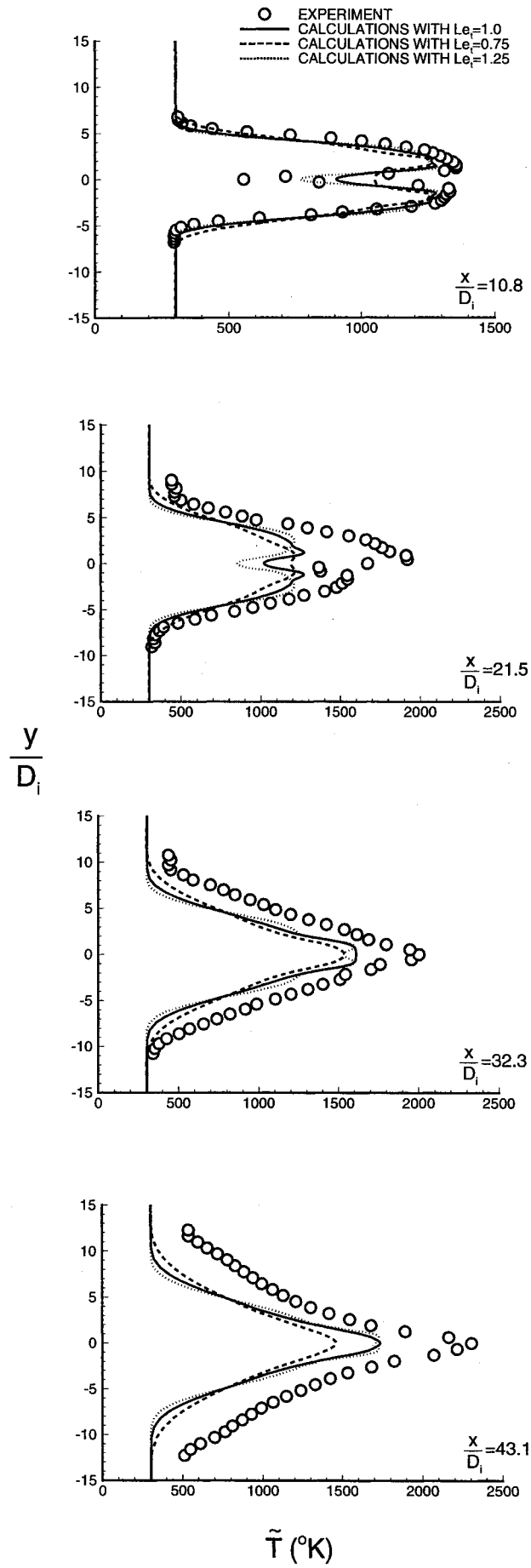

Fig. 19 Computed mean temperature profiles for various turbulent Lewis numbers compared with experiment.

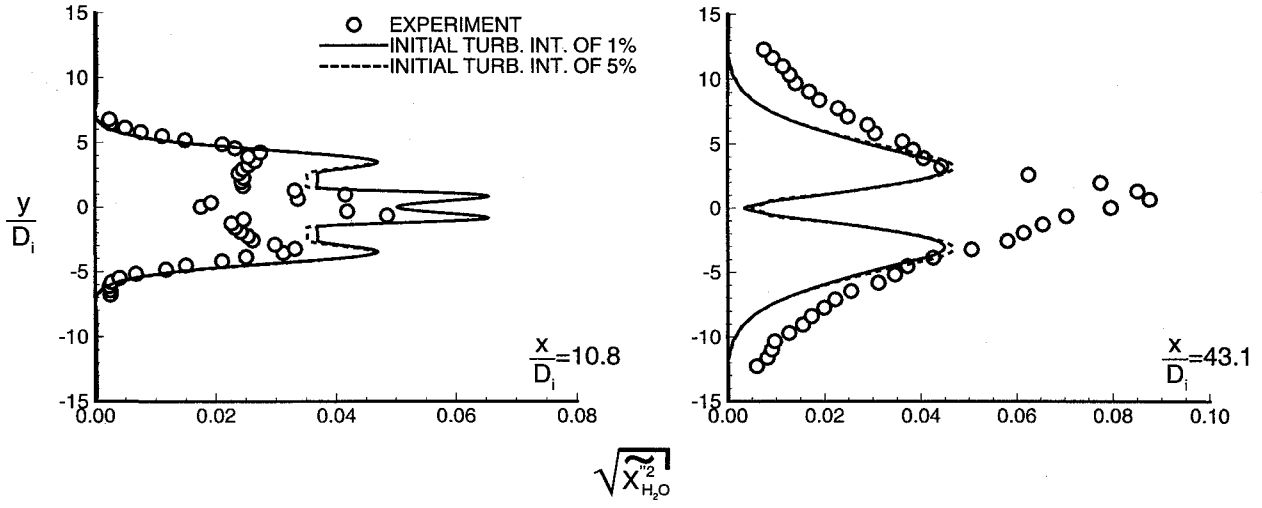

Fig. 20 Computed rms H_2O mole fraction profiles for various turbulent Lewis numbers compared with experiment.

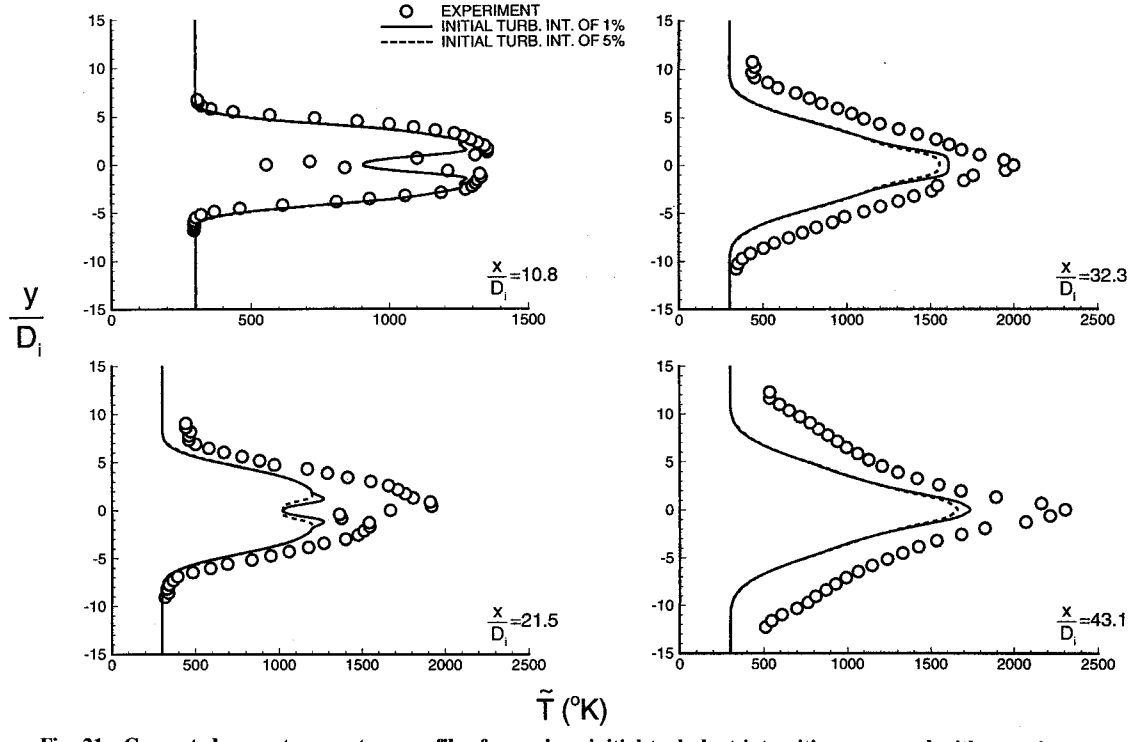

Fig. 21 Computed mean temperature profiles for various initial turbulent intensities compared with experiment.

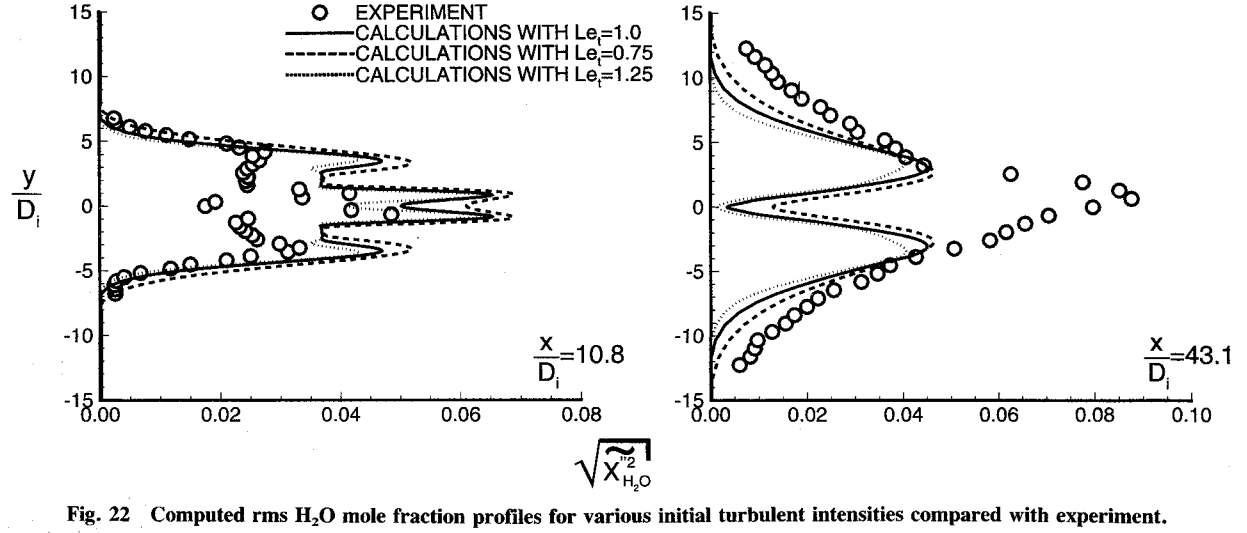

Fig. 22 Computed rms H_2O mole fraction profiles for various initial turbulent intensities compared with experiment.

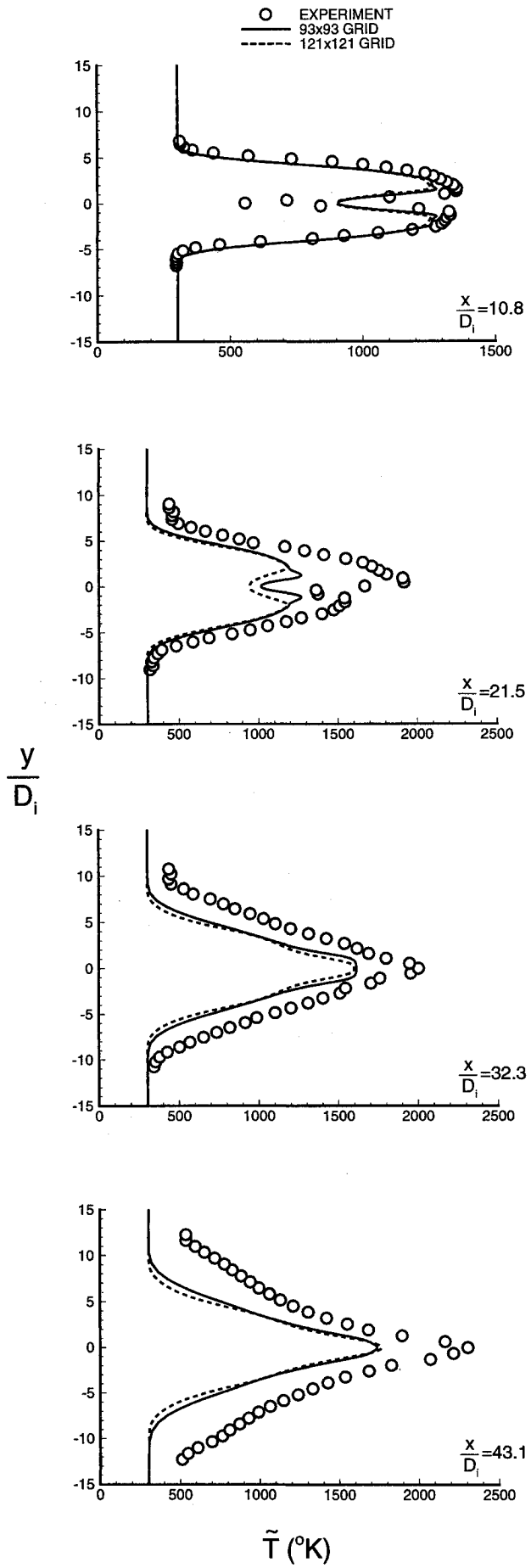

Fig. 23 Computed mean temperature profiles for various grid geometries compared with experiment.

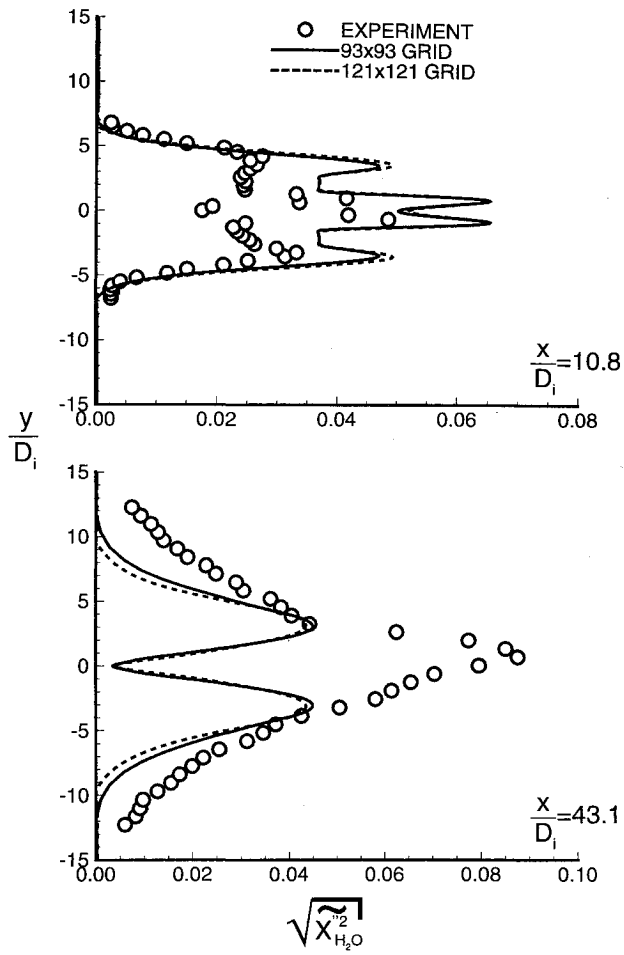

Fig. 24 Computed rms H_2O mole fraction profiles for various grid geometries compared with experiment.

Concluding Remarks

Based on present calculations and comparisons with experiment, it appears that the multivariate Beta PDF of Girimaji is well suited for studying mixing, but may not be suited for studying combustion. It is possible that a more elaborate PDF will result in improved predictions. The present calculations point the need for addressing differences between Favre and time averaging. For problems involving supersonic flows, the difference may be significant so that it may not be possible to have a meaningful comparison between theory and experiment. A sensitivity study of the various model constants and turbulent intensity exiting the nozzle did not modify the above conclusions.

Acknowledgments

This work is supported in part by the following grants: NASA Grant NAG-1-244 and the Mars Mission Center funded by NASA Grant NAGW-1331. The authors would like to express their appreciation to S. S. Girimaji for many helpful discussions.

References

[1]Cheng, T. S., Wehrmeyer, J. A., Pitz, R. W., Jarrett, O., Jr., and Northam, G. B., "Finite-Rate Chemistry Effects in a Mach 2 Reacting Flow," AIAA Paper 91-2320, June 1991.

[2]Pope, S. B., "PDF Methods for Turbulent Reacting Flows," *Progress in Energy Combustion Science*, Vol. 11, 1985, pp. 119–192.

[3]Bilger, R. W., "Turbulent Flows with Nonpremixed Reactants," *Turbulent Reacting Flow, Topics in Applied Physics*, edited by P. A. Libby and F. A. Williams, Vol. 44, Springer-Verlag, Berlin, 1980, pp. 65–113.

[4]Jachimowski, C. J., "An Analytic Study of the Hydrogen-Air

Reaction Mechanism with Application to Scramjet Combustion," NASA TP 2791, Feb. 1988.

[5]Girimaji, S. S., "A Simple Recipe for Modeling Reaction-Rates in Flows with Turbulent Combustion," AIAA Paper 91-1792, June 1991.

[6]Eklund, D. R., Drummond, J. P., and Hassan, H. A., "Numerical Modeling of Turbulent Supersonic Reacting Coaxial Jets," *AIAA Journal*, Vol. 28, No. 9, 1990, pp. 1633–1641.

[7]Frankel, S. H., Drummond, J. P., and Hassan, H. A., "A Hybrid Reynolds Averaged/PDF Closure Model for Supersonic Turbulent Combustion," AIAA Paper 90-1573, June 1990.

[8]Baurle, R. A., Drummond, J. P., and Hassan, H. A., "An Assumed PDF Approach for the Calculation of Supersonic Mixing Layers," AIAA Paper 92-0182, Jan. 1992.

[9]Baurle, R. A., Alexopoulos, G. A., and Hassan, H. A., "An Assumed Joint-Beta PDF Approach for Supersonic Turbulent Combustion," AIAA Paper 92-3844, July 1992.

[10]Narayan, J. R., and Girimaji, S. S., "Turbulent Reacting Flow Computations Including Turbulence-Chemistry Interactions," AIAA Paper 92-0342, Jan. 1992.